ACS OMEGA

Article

Cite This: ACS Omega 2017, 2, 8810−8817

Reversible Tuning of Ferromagnetism and Resistive Switching in ZnO/Cu Thin Films

Muhammad Younas,*[,†,‡] Chi Xu,[§] Muhammad Arshad,[∥] Lok Ping Ho,[†] Shengqiang Zhou,[§] Fahad Azad,[†,⊥] Muhammad Javed Akhtar,[‡] Shichen Su,[†] Waqar Azeem,[†] and Francis C. C. Ling*[,†]

[†]Department of Physics, The University of Hong Kong, Pokfulam Road, Hong Kong 999077, China

[‡]EMMG, Physics Division, PINSTECH, P.O. Nilore, Islamabad 45650, Pakistan

[§]Helmholtz-Zentrum Dresden-Rossendorf, Institute of Ion Beam Physics and Materials Research, Bautzner Landstrasse 400, 01328 Dresden, Germany

[∥]Nanoscience and Technology Department, National Centre for Physics, Quaid-i-Azam University, Islamabad 45320, Pakistan

[⊥]School of Natural Sciences, National University of Sciences and Technology (NUST), 44000, H-12, Islamabad, Pakistan

ABSTRACT: Systematic magnetic, electronic, and electrical studies on the $Cu_{0.04}Zn_{0.96}O/Ga_{0.01}Zn_{0.99}O$ cell structure grown on (001) sapphire by the pulsed laser deposition technique show that the Cu multivalent (Cu^{M+}) ions modulate magnetic and resistive states of the cells. The magnetic moment is found to be reduced by ∼30% during the high resistance state (HRS) to low resistance state (LRS) switching. X-ray photoelectron spectroscopy results reveals an increase of the Cu^{+}/Cu^{2+} oxidation state ratio (which has been determined by the relative positions of the Fermi level and the Cu acceptor level) during the HRS to LRS transition. This decreases the effective spin-polarized $Cu^{2+}-V_{ö}-Cu^{+}$ channels and thus the magnetic moment. A conduction mechanism involving the formation of conductive filaments from the coupling of the Cu^{M+} ions and $V_{ö}$ has been suggested.

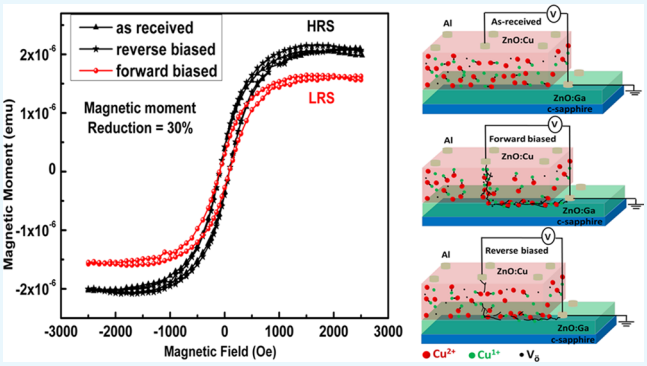

1. INTRODUCTION

Tuning magnetic properties by external means without varying temperature would be highly anticipated from fundamental and technological perspectives. It has been a long quest to regulate the magnetic properties of solids by electric fields. Voltage-induced magnetic modulations can be much more dynamically efficient than that of magnetic fields or spin-polarized currents. The electric-field manipulation of magnetism is of major concern not only because of its technological significance but also because it motivates to reveal properties of magnetic materials that are otherwise inaccessible. Similarly, electrically controlled resistive switching (RS) has potential applications in resistive switching random access memory (RRAM), which is a promising candidate for next-generation nonvolatile memory devices. RRAM is generally modulated by electrical stimulus for the recording of "0" and "1" logic states by changing resistance modes of the material under observation.[1,2] Simultaneous control on magnetism and resistance of single-phase materials can be much beneficial for spintronic devices. In such devices, an external field switches resistance between a high resistance state (HRS) and low resistance state (LRS), which in turn modulates magnetic properties in a reversible and nonvolatile manner.[3−7]

ZnO is an academically curious material and has been much celebrated from both fundamental understanding and application points of view. In addition to the excellent optoelectronic properties, it has been demonstrated that both undoped and transition metal doped ZnO systems show coexistence of resistive and magnetic switching under an applied electric field when sandwiched between Ti, Pt, Au, indium tin oxide glass, and $SrRuO_3$ electrodes.[8−11] In these systems, electric and magnetic modulations are generally derived, either by metal electrodes or by the oxide formation at the interface. Growth of ZnO films on a metal or structurally different material introduces defects thereby suppressing the actual role of the ZnO matrix. ZnO would be more appropriate for applications once the metallic electrodes can be replaced with a similar crystal structure as that of ZnO. It would also be useful from the processing perspective if the electrodes and the dielectric layers are based on a single material system. Gallium-doped ZnO films show metallic conductivity with the Fermi level position above the conduction band edge of ZnO and, therefore, can be much better replacement for metal electrodes.[12]

To avoid magnetic oxide formation at the interface, selection of nonmagnetic elements can be of good use. The ZnO/Cu

Received: August 16, 2017
Accepted: November 2, 2017
Published: December 8, 2017

DOI: 10.1021/acsomega.7b01192
ACS Omega 2017, 2, 8810−8817

thin film is a potential candidate for resistive switching properties.[5] The Cu dopant is important because neither metallic Cu nor its oxides are ferromagnetic at room-temperature.[13] Ferromagnetism (FM) can arise in the ZnO/Cu system because of certain types of defect states. Point defects such as oxygen vacancy ($V_{\ddot{o}}$), Cu–$V_{\ddot{o}}$, Cu^{M+} ions, and electrochemical reduction of Cu play vital roles in controlling RS and FM in the ZnO/Cu system.[14−16] Therefore, mutual FM and RS in the single phase ZnO/Cu material would be interesting from application and fundamental understanding points of view. Different models have been suggested to interpret the RS mechanism including charge trapping/detrapping,[16,17] conductive filament formation/rupture controlled either by thermal effects[18] or by electrochemical redox reactions.[7,19,20] Although the electrochemical redox reaction-regulated filament is much celebrated, there is still lack of systematic study to reveal the actual role of the redox reaction in tuning RS and FM in ZnO/Cu thin films. Therefore, we have performed comprehensive *I*−*V*, magnetization, and X-ray photoelectron spectroscopy (XPS) analyses to understand the magnetic and resistive switching properties of ZnO/Cu thin film-based cell structure.

2. RESULTS AND DISCUSSION

In the present study, Al/$Cu_{0.04}Zn_{0.96}O$/$Ga_{0.01}Zn_{0.99}O$/c-sapphire were grown using the pulsed laser deposition method (as shown in the inset of Figure 1) with the oxygen pressure of

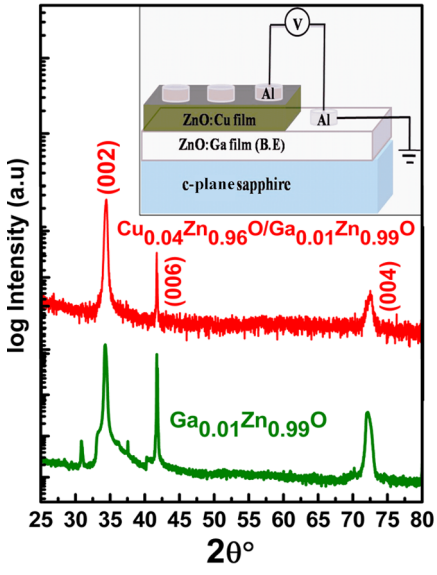

Figure 1. XRD of the $Cu_{0.04}Zn_{0.96}O$/$Ga_{0.01}Zn_{0.99}O$/(001) sapphire and $Ga_{0.01}Zn_{0.99}O$/(001) sapphire. Inset shows the schematic of the cell structure.

$P(O_2)$ = 0.02 Pa. In a previous study,[21] we have systemically studied $Cu_{0.04}Zn_{0.96}O$ films grown on c-sapphire and found that growing the samples at $P(O_2)$ = 0.02 Pa yielded the films with good epitaxial quality and largest magnetization. The X-ray diffraction (XRD) spectrum (with diffraction intensity in log scale) of the $Cu_{0.04}Zn_{0.96}O$ grown on top of $Ga_{0.01}Zn_{0.99}O$ and that of bare $Ga_{0.01}Zn_{0.99}O$ films are shown in Figure 1. Other than (002) and (004) peaks of wurtzite ZnO and the (006) peak of sapphire, no other peak is found. The as-received structures are single phase, and comparatively lower (002) peak intensity of $Cu_{0.04}Zn_{0.96}O$ than that of $Ga_{0.01}Zn_{0.99}O$ may be related to the degraded epitaxial quality because of Cu doping.[21] Hall effect measurements performed on the bare $Ga_{0.01}Zn_{0.99}O$ film yielded a degenerately high electron concentration of 2 × 10^{20} cm^{-3} and a low resistivity of (~5 × 10^{-4} Ω cm). The Ohmic behavior of the bare $Ga_{0.01}Zn_{0.99}O$ film was also confirmed by *I*−*V* measurements. The $Ga_{0.01}Zn_{0.99}O$ film serves as the bottom electric contact and the $Cu_{0.04}Zn_{0.96}O$ film grown on top of it could have a better epitaxial quality because both the $Cu_{0.04}Zn_{0.96}O$ and $Ga_{0.01}Zn_{0.99}O$ films have the same ZnO wurtzite structure.

For the *I*−*V* measurements, we first tested sweeping voltages of magnitude ±2 and ±4 V to analyze any transition and memory effects in the *I*−*V* characteristics of the designed cell structure as shown in Figure 2. The sweep voltages were

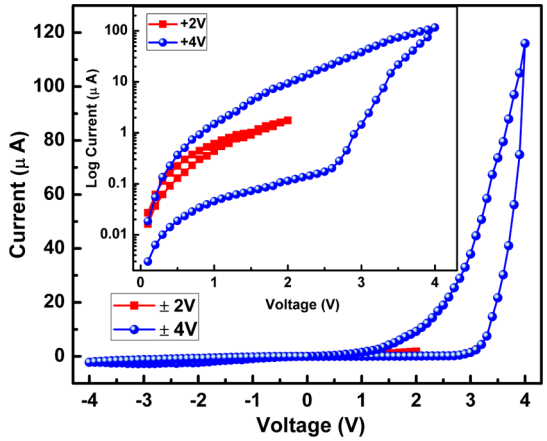

Figure 2. *I*−*V* curves for the $Cu_{0.04}Zn_{0.96}O$/$Ga_{0.01}Zn_{0.99}O$/(001) sapphire cell structure collected under different sweeping voltages. Inset shows log *I* vs *V* memory effect for the same structure collected under different positive voltage regions only.

applied to the top electrode of the Al/$Cu_{0.04}Zn_{0.96}O$/$Ga_{0.01}Zn_{0.99}$/(001) sapphire structure in the sequence 0 → +V → 0 → −V → 0, whereas the bottom electrode of the Al/$Ga_{0.01}Zn_{0.99}$/(001) sapphire structure were grounded. For the fresh cell structure, the original state is HRS. We observe smooth transitions in the *I*−*V* curves without the electroforming process under two sweeping voltages. Electroforming is a pretreatment process to decrease the cell's resistance by several orders via formation of conducting filaments in the insulating matrix and is considered as a serious obstacle in realizing high-density RRAM devices. One of the substantial importances of the present cell structure is its avoidance of the electroforming process under sweeping voltages of different magnitudes. Figure 2 shows that for the tested sweeping voltages, current rises steadily only in the positive voltage regions, whereas in the negative voltage regions, the current is extremely low and the cell structure remain in the HRS. Comparatively, ±2 V sweeping voltage shows negligible transitions in the *I*−*V* curves without any memory effect (inset in Figure 2) revealing that the applied sweeping voltage is not sufficient enough to change the resistance states of the cell structure. On the other hand, ±4 V sweeping voltage demonstrates high transition in the *I*−*V* curves along with observable memory effects (inset in Figure 2).

The preliminary *I*−*V* analysis shows that the application of ±4 V sweeping voltage to the cell structure gives smooth *I*−*V* transitions with a noticeable memory effect. Therefore, we

DOI: 10.1021/acsomega.7b01192
ACS Omega 2017, 2, 8810−8817

employed ±4 V sweeping voltage to analyze the resistive switching behavior and magnetic modulation effects in the present cell structure. The ±4 V sweep voltage was applied to the Al/$Cu_{0.04}Zn_{0.96}O$/$Ga_{0.01}Zn_{0.99}O$/(001) sapphire (top electrodes) in the sequence 0 → +4 V → 0 → −4 V → 0, whereas the Al/$Ga_{0.01}Zn_{0.99}O$/(001) sapphire (bottom electrodes) were grounded. Figure 3 shows that when ±4 V sweep voltage is

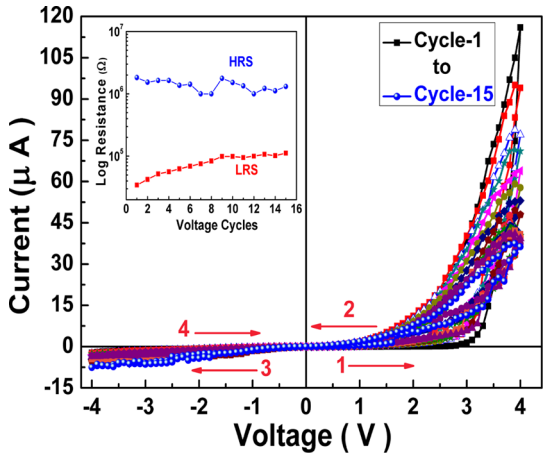

Figure 3. Multiple *I*−*V* curves for the $Cu_{0.04}Zn_{0.96}O$/$Ga_{0.01}Zn_{0.99}O$/(001) sapphire cell structure. Arrows show the direction of sweeping voltages. Inset shows log resistance vs voltage cycles for the same cell structure.

applied in multiple loops, the *I*−*V* plot retraces itself in both sweep directions. For very first sweeping cycle, when the positive voltage imposed on the cells increases steadily, a pronounced rise in current ($\sim 10^{-4}$ A) is observed at $V \approx +4$ V and the cells switch to LRS. The LRS is retained (ON state) during sweeping back of voltage from +4 V till negative voltage sweep (0 → −4 V → 0), at which the current switches to extremely low current $\sim 10^{-6}$ A (OFF state). During the second sweeping cycle, the ON state is again achieved only for the positive sweeping voltage but the LRS current at a voltage decreases to 9×10^{-5} A. Similarly, the LRS current at a voltage reduces to 3×10^{-5} A till the 15th sweeping cycle. However, the voltage required to achieve LRS current remains the same for all sweeping cycles. For the endurance test (inset in Figure 3), the resistance values were measured at ±4 V reading voltage in each dc sweep. Resistance values for LRS show increasing trends against sweeping cycles, whereas those of HRS are scattered. Although the HRS values are somewhat fluctuant, the HRS/LRS ratios are still in the range of $\sim 10^2$ over 15 cycles. These observations show that the LRS state retains itself until the negative voltage is applied to tune the cells to their initial HRS (which is indeed a memory effect) and shows very low current indicating that Cu doping suppresses HRS current efficiently.

Noticeable opening in the *I*−*V* curves (Figure 2) suggests the possible memory effect of the measured cell structure rather than the rectification characteristics. To further ensure the memory effect, the cells were switched to LRS by +4 V and the electrical bias was then detached. Then, *I*−*V* measurement was then performed with a much smaller bias (0.3−0.5 V). Similarly, we switched the cells to HRS by employing −4 V and then detaching the electrical bias. *I*−*V* measurement was then carried out with a smaller bias. The results are shown in Figure 4. We observe a clear bifurcation in the *I*−*V* curves of

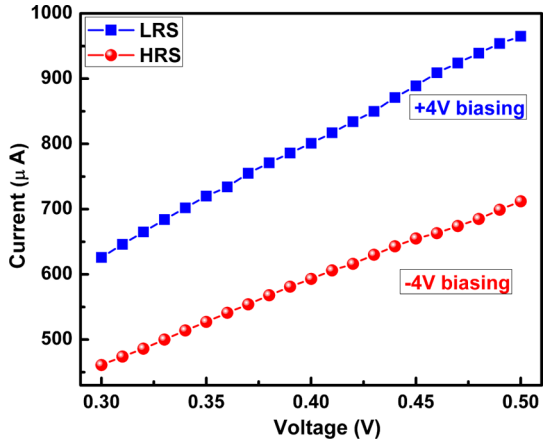

Figure 4. *I*−*V* curves for the $Cu_{0.04}Zn_{0.96}O$/$Ga_{0.01}Zn_{0.99}O$/(001) sapphire cell structure after biasing with +4 V and −4 V. The cell was switched to LRS (HRS) by +4 V (−4 V), and then, the electric bias was detached. The *I*−*V* measurement was then carried out, and the results are shown in the figure. Difference between the LRS and HRS current shows memory effect of the cell structure.

LRS and HRS indicating memory behavior of the cell structure. In effect, the sample retains its LRS and HRS until respective states can be swapped by the application of negative and positive voltages, respectively. Thus, with the +4 V pulse we can "write" the LRS and subsequently the −4 V pulse "erases" the high conducting state and recalls the initial HRS. The *I*−*V* characteristics measured at different cells on the film were almost identical in nature showing a high degree of reproducibility.[22] However, after the positive bias is detached, one of the reasons of the quick drop in the current during subsequent cycles is due to variable locations and orientations of the residual conducting filaments. This behavior is also shown in the inset of Figure 3 by the scattered HRS values and increasing trends of the resistance of LRS against sweeping voltage cycles.

In the upcoming section, the effects of RS on magnetic variations of the cell structure will be discussed, which is the main exploration of this work. Previously, we have studied the ZnO/Cu thin films grown under different oxygen partial pressures.[21] This study highlighted correlation among the magnetization, $V_{ö}$ defects, and Cu^{M+} ions. Each $V_{ö}$ was found to introduce one large size localized orbital and two doped electrons. The dopant-defect hybridization generates ferromagnetically aligned Cu^{2+}−$V_{ö}$−Cu^{+} networks, and a long range ferromagnetic order would develop in the ZnO/Cu thin films.[21,23] Detailed XRD, XPS, and high resolution transmission electron microscopy, and magnetization studies suggested that thin film quality played a less effective role in governing the magnetic properties. Instead, room temperature FM of ZnO/Cu thin film samples are highly tunable by the simultaneous presence of CuO nanophases and multivalent Cu and $V_{ö}$ concentrations, which are in strong contest with each other.[21] For vacuum ($P(O_2)$ = 0.0 Pa)-grown thin film samples containing a high $V_{ö}$ concentration and Cu^{+} as the dominant oxidation state, the Cu^{2+}−$V_{ö}$−Cu^{+} network became ineffective and a CuO nanophase (4−5 nm) was the dominant FM supplier. In case of high oxygen partial pressure ($P(O_2)$ = 1.00 Pa) grown sample, the observed FM was very weak and distorted. The high oxygen supply during thin film growth introduced relatively larger size nanophases (8−10 nm) of CuO and created a substantial decrease in the $V_{ö}$ concentration

DOI: 10.1021/acsomega.7b01192
ACS Omega 2017, 2, 8810−8817

resulting in a comprehensive reduction of the Cu^{2+}–$V_ö$–Cu^+ network. Moreover, we observe that the low oxygen pressure (i.e. $P(O_2)$ = 0.02 Pa) is important during thin film growth to get enhanced magnetic properties. Withholding $P(O_2)$ = 0.02 Pa during thin film growth, introduces sufficient amount of $V_ö$ with a dominant Cu^{2+} oxidation state thereby producing effective Cu^{2+}–$V_ö$–Cu^+ networks as major contributors to FM. On the other hand, the CuO nanophases if they exist play a less important role in tuning FM. Therefore, this is one of the primary motivations for the growth of the present cell structure under $P(O_2)$ = 0.02 Pa.

The capability of the present cell structure to retain the resistive states allows one to disconnect the sample from the electrical circuit and measure the magnetization loop. We have carried out RS-induced magnetic measurement for the as-received state, HRS, and LRS of the cells as representatively displayed in Figure 5. We first measured room temperature

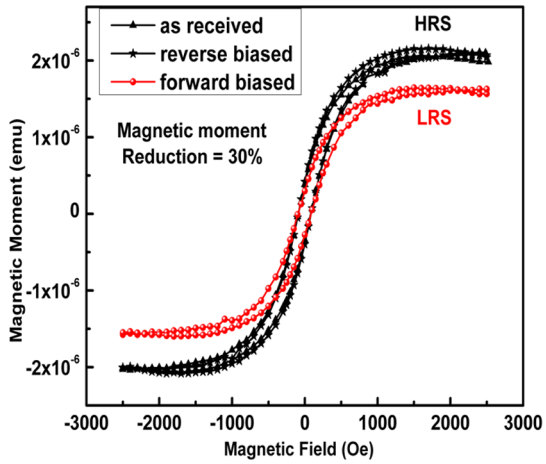

Figure 5. Room temperature MH loops of the $Cu_{0.04}Zn_{0.96}O$/$Ga_{0.01}Zn_{0.99}O$/(001) sapphire for the as-received, forward-biased, and reverse-biased states.

magnetization on the as-received cell structure without any biasing. To observe the RS-induced FM, all the cells were switched to the LRS by applying +4 V. Subsequently, magnetization showed the magnetic moment reduction of 30% in the LRS of the cells. Then, *I*–*V* measurements with a much smaller bias (0.3–0.5 V) on some of the cells showed that they were in the LRS. To check the reversibility of the magnetic switching, every cell was switched back to the HRS by employing −4 V and magnetization was reperformed. Indeed, the magnetic moment can be recovered, indicating reversible control on magnetism by an electric bias. It should be noted here that every time the sample was disconnected from the circuit before execution of magnetic measurements.

We will now explore the possible origin of ferromagnetic modulations by electrical biasing. The Cu acceptor level (0/−) lies 0.18–0.2 eV below the conduction-band minimum (CBM). The (0/−) refers to the change of the charge state of the Cu from neutral to negatively charged by losing a hole. The (0/−) ionization state referred to the transition of Cu^{2+} to Cu^+ as the Fermi level moves over the (0/−) level, while the Cu^+ charge state is located at 0.390 eV above the valence band.[24−26] Recently, charge state switching of Cu acceptors in ZnO nanorods was observed by the rise in the Fermi level above the 0/− (Cu^{2+}/Cu^+) charge transfer level as a result of Ga donor dopant introduction.[26] Therefore, within the similar framework, the possibility of changing the Fermi energy level by the electric field effect can clarify the real nature of the electronic band structure of the ZnO/Cu-based cell structure. Thus, in the present study of the ZnO/Cu thin film, the E_F positions during HRS and LRS were estimated by the equation, $n = N_c \exp(E_F - E_C/kT)$ and $n = \sigma/e\mu_e$, where n is the carrier concentration, N_c is the effective density of states at 300 K for ZnO (3.9×10^{18} cm^{-3}), σ is the conductivity, and μ_e is the electron mobility for the $Cu_{0.04}Zn_{0.96}O$ thin film at 300 K (30 cm^2 V^{-1} s^{-1}).[27,28] The E_F values were found to be about 0.34 and 0.15 eV below the CBM during HRS and LRS, respectively.

From the above discussion, we can infer the existence of Cu^{M+} ions and a higher Cu^+/Cu^{2+} ratio during the transition from the HRS to LRS because of the rise in the Fermi level. Along with Cu^{M+} ions, there is sufficient amount of $V_ö$ as the cell structure were grown under low $P(O_2)$ = 0.02 Pa. According to the first-principles calculation, each $V_ö$ introduces one large size localized orbital and two doped electrons. The doped electrons associated with the $V_ö$ would spill over the 3d orbitals of the surrounding Cu^{M+} ions, making them closer to Cu^+.[14] Therefore, we propose that the observed FM in the as-received cells are attributed to the coupling between the electron trapped by $V_ö$ and Cu^{M+} ions via Cu^{2+}–$V_ö$–Cu^+ networks. Under magnetic field, the spin-polarized Cu^{2+}–$V_ö$–Cu^+ channels get aligned and generate FM. During LRS, moving up of the E_F level over the Cu (0/−) level converts Cu^{2+} to Cu^+, which resulted in the decrease of effective spin-polarized Cu^{2+}–$V_ö$–Cu^+ channels and thus reduction in FM (∼30%). During HRS, moving down of the E_F level results in more abundant Cu^{2+} ions. These Cu^{2+} ions would generate effective spin-polarized Cu^{2+}–$V_ö$–Cu^+ channels and FM switches back to the original value. To further investigate the existence of Cu^{M+} ions and their interaction with $V_ö$ in the form of Cu^{2+}–$V_ö$–Cu^+ defect complex, XPS measurements can be much beneficial.

The detailed XPS analysis has been performed during different states of the cell structure. First, XPS was performed on the as-received cell structure without any biasing. To observe electrically induced changes in XPS spectra, all the cells were switched to the LRS with forward biasing of +4 V, and subsequently, XPS data were collected. To check the reversibility of the XPS spectra, every cell was switched back to the HRS by employing reverse biasing of −4 V, and XPS data were collected again. Before the XPS measurements, the LRS and HRS features were carefully checked with similar measurements as shown in Figure 4, and the XPS measurements were conducted with the electric bias detached. XPS survey scans for the as-received state, LRS, and HRS of the cells are presented in Figure 6. Only Zn, Cu, O, and C elements and no additional peak related to Al or other elements were detected. The XPS spectra for the as-received cells in Figure 7 indicate Cu $2p_{3/2}$, Cu $2p_{1/2}$, and satellite peaks. After setting every cell to LRS, the Cu 2p peak intensities reduce and the satellite peaks disappear. While resetting the sample to HRS, Cu 2p peaks regain original intensities and satellite peaks reappear (insets in Figure 7). For all three states of the cells, the Cu $2p_{3/2}$ (933.15–933.22 eV) and Cu $2p_{1/2}$ (953.05–953.11 eV) peak positions show Cu^{M+} ions.[29−31] Therefore, each XPS spectrum is deconvolved into Cu^{2+} and Cu^+ components. The fittings are accomplished by using Cu^{2+} and Cu^+ components (corresponding to the Cu 2p peak positions of Cu^{2+} in CuO and Cu^+ in Cu_2O).[29,32] By employing XPS integrated areas and Cu $2p_{3/2}$/Zn $2p_{3/2}$ ratio, we obtained Cu atomic % of 0.5, 0.3,

DOI: 10.1021/acsomega.7b01192
ACS Omega 2017, 2, 8810–8817

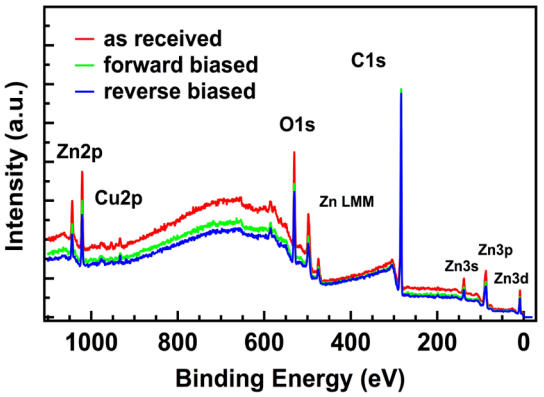

Figure 6. Survey scans for the as-received, forward-biased (LRS), and reverse-biased (HRS) states of the $Cu_{0.04}Zn_{0.96}O/Ga_{0.01}Zn_{0.99}O/(001)$ sapphire cell structure.

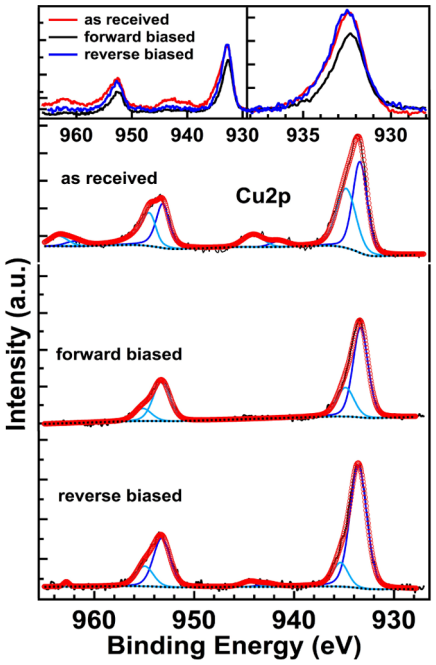

Figure 7. Core level Cu 2p XPS fitting spectra of the $Cu_{0.04}Zn_{0.96}O/Ga_{0.01}Zn_{0.99}O/(001)$ sapphire for the as-received, forward-biased, and reverse-biased states of the cell structure. Insets show Cu 2p XPS spectra of the cells without fitting.

and 0.45 for as-received, forward-biased, and reverse-biased states of the cells, respectively. The fitting results are presented in Table 1.

Satellite peaks are commonly found between 940−945 eV for Cu^{2+}, and no satellite peaks are expected for the Cu^0 and Cu^+ states.[33] The CuO is normally characterized by broader and high-intensity satellite peaks at ∼10 eV higher binding energy from the main Cu 2p peaks.[21] Satellite peaks ∼9.1−7.9 eV from the main Cu 2p peaks suggest the absence of the CuO phase; therefore, Cu^{2+} is the more dominant oxidation state in the as-received cells. During LRS, the abundant Cu^{2+} surface ions drift down to the bottom electrode and convert to Cu^+ after capturing injected electrons. This is in agreement with upmove of E_F during LRS of the cells because of interactions of injected carriers with Cu^{2+} ions. These Cu^{2+} and Cu^+ ions couple with $V_{ö}$ efficiently to form $Cu^{2+}-V_{ö}-Cu^+$ networks, which is essentially a process of electrochemical redox reactions.[7] The redox reaction is not through Cu movement, instead electron transfers between Cu^{2+} and Cu^+ via $V_{ö}$. The $Cu^{2+}-V_{ö}-Cu^+$ defect complexes connect with each other to form networks and facilitate formation of Cu-based filaments along conduction paths. These conduction paths set the cells into LRS, thereby reducing Cu atomic % to 0.3 at the surface. During reverse biasing, the locally connected $Cu^{2+}-V_{ö}-Cu^+$ networks are disrupted because of the lack of injected carriers, and the sample was reset into HRS. At the surface, the Cu atomic % regains the original value (0.45%) as that of the as-received cell structure (0.5%) and results in a higher Cu^{2+}/Cu^+ ratio. This is again in consonance with the down shift in E_F during HRS of the cells.

To further understand the effects of $V_{ö}$ on the bonding nature of oxygen with Cu^{M+} ions, we performed O 1s XPS analysis as presented in Figure 8. The irregular features in the O 1s spectra are divided into subspectral components.[34] The O2 and O3 peak intensities remain quite the same. However, the O1 peak intensity progressively declines during forward and

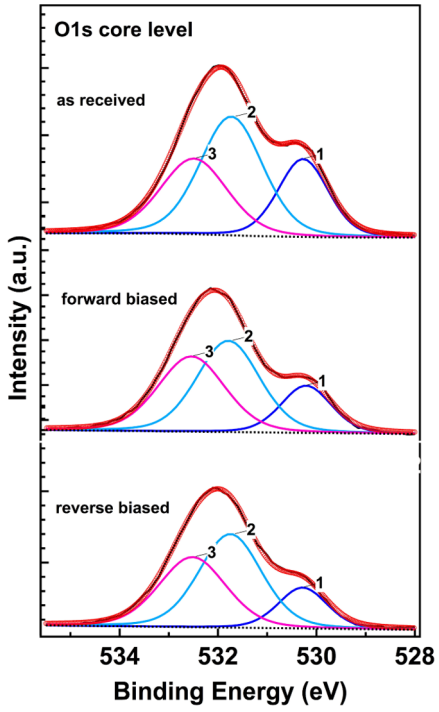

Figure 8. Core level O 1s XPS fitting spectra of the $Cu_{0.04}Zn_{0.96}O/Ga_{0.01}Zn_{0.99}O/(001)$ sapphire for the as-received, forward-biased, and reverse-biased states of the cell structure.

Table 1. XPS Fitting Parameters for $Cu_{0.04}Zn_{0.96}O/Ga_{0.01}Zn_{0.99}O/(001)$ Sapphire Cells under Different States

cell structure	Cu-atomic %	Cu $2p_{3/2}$ (eV)	Cu $2p_{1/2}$ (eV)	satellite peak (eV)	Cu^+/Cu^{2+}	relative $V_{ö}$ strength %
as-received	0.50	933.22	953.11	942.30	4.4	45
forward-biased (LRS)	0.30	933.15	953.05	nil	6.9	44
reverse-biased (HRS)	0.45	933.21	953.06	942.30	4.6	46

DOI: 10.1021/acsomega.7b01192
ACS Omega 2017, 2, 8810−8817

reverse biasing. This shows change in the typical behavior of O ions organized in a wurtzite lattice of hexagonal Zn^{2+} ions at the surface because of application of high voltage. By employing integrated areas of O1, O2, and O3 peaks, relative strength of O2 (i.e., $V_{ö}$) is estimated (see Table 1). Setting cells to LRS stimulates an observable change in the Cu-oxidation states rather than $V_{ö}$ in the regions around the conducting filament, which can be easily detected by XPS. In addition, most of the Cu^{M+} ions and $V_{ö}$ are utilized in the formation of Cu^{2+}–$V_{ö}$–Cu^{+} defect complexes, and these isolated networks accumulate along the conducting path to form the filament (Figure 9). This

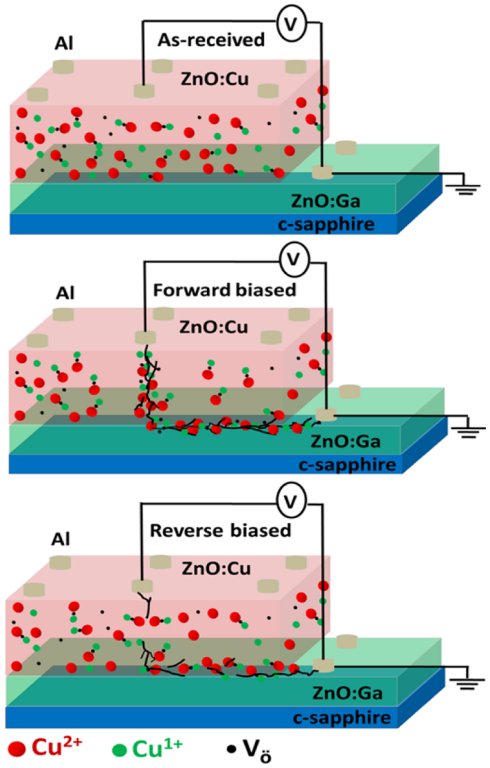

Figure 9. Schematic representations of the conducting filament process for the as-received, forward-biased, and reverse-biased states of the cell structure.

process occurs at the expense of reduction in the isolated spin-polarized Cu^{2+}–$V_{ö}$–Cu^{+} networks in the close proximity of the conducting filament and magnetic moment reduced to 30%. During HRS of the cells, the conducting filament ruptures (Figure 9) and isolated Cu^{2+}–$V_{ö}$–Cu^{+} effective networks are available again in the matrix of the ZnO/Cu thin films to tune the reduced magnetic moments to their original higher values. It seems here that change in the status of cells can create imbalance of the isolated spin-polarized Cu^{2+}–$V_{ö}$–Cu^{+} networks within the matrix of the $Cu_{0.04}Zn_{0.96}O$ film. From the present investigation of magnetic and XPS analyses, it has been observed that during biasing of the cells, $V_{ö}$ contents remain fixed and change in Cu^{2+}/Cu^{+} ratios tune magnetic and electronic properties.

In the RS of ZnO, the $V_{ö}$ has been known to play a dominant role in controlling the conducting filament.[35] Joule heating is considered responsible for the rupture of $V_{ö}$-based filament and results in a sharp transition from LRS to HRS of the cells. We observe smooth RS and found that the Cu^{2+} acceptor level can combine efficiently with $V_{ö}$, which in turn impedes isolated $V_{ö}$ gathering at the interface.[24,25] Moreover, absence of the electroforming process excludes the possible role of $V_{ö}$ to start the RS modulations.[1] The already existed Cu^{2+} cations in the as-received cells effectively save the relatively long-term oxidation of Cu atoms at the anode in the very first cycle. In addition, the average drift distance between Cu^{2+} ions and the cathode is shortened because of the electron transfer between Cu^{2+} and Cu^{+} via $V_{ö}$ orbitals. Both these phenomena accelerate the formation of Cu^{2+}–$V_{ö}$–Cu^{+} networks along the conduction path and result in avoidance of the electroforming process.[7] These observations suggest that the conducting filament is not based on the isolated $V_{ö}$, other entities might also be involved. Hence, it is considered that rupture/formation of the conducting filament might be due to the electrochemical redox reactions of doped Cu in ZnO.[7]

To further investigate the origin of RS, all the cells were forward-biased (0 → +4 V → 0), and subsequently, we performed nonlinear fittings to I–V curves (Figure 10) in the

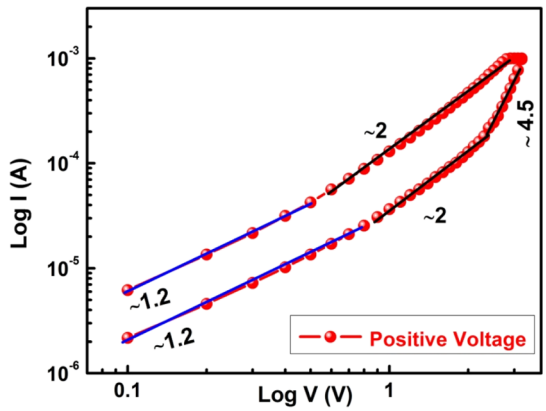

Figure 10. log I vs log V for the $Cu_{0.04}Zn_{0.96}O/Ga_{0.01}Zn_{0.99}O/(001)$ sapphire. Solid lines are best fit to the data.

positive voltage regions. The I–V curves seem to follow Ohmic conduction, trap-controlled space charge limited current (SCLC), and Poole–Frenkel (P–F) emission mechanisms in different voltage regions. In the SCLC, the I–V curve first conforms the Ohmic conduction ($I \propto V$) and then Child's law ($I \propto V^2$).[33,36] At lower voltage (slope ≈ 1.2), current flowing through the cell is mainly intrinsic and can be explained by the Ohmic conduction model. With further increase in the voltage (slope ≈ 2), the injected carriers become predominant, and an increase in current obeys Child's law ($I \propto V^2$). Once all of the traps are filled, a rapid increase in current is observed at a higher voltage (slope ≈ 4.5), which is regarded as P–F emission of electrons.[37] After P–F emission, the filament is formed because of the gathering of Cu^{M+} ions and $V_{ö}$ along the conducting path and the cells switch from HRS to LRS. During reverse biasing of the cells (0 → −4 V → 0), already filled defect states exhaust the trapped charges as there is no extra supply of injected carriers. In this way, already assembled Cu^{M+} ions and $V_{ö}$ along the conducting path start dispersing and fuses the conducting filaments, thereby switching the LRS of the cells back to HRS under the negative bias. During subsequent cycles, the I–V behavior is nonuniform and the cells become more resistive because of fluctuating locations and orientations of the residual conducting filaments.

DOI: 10.1021/acsomega.7b01192
ACS Omega 2017, 2, 8810–8817

3. CONCLUSIONS

From the present study, it can be concluded that we can electrically tune the magnetic state of the cell structure for which ferromagnetically aligned Cu^{2+}−$V_{ö}$−Cu^{+} networks are considered responsible in altering the magnetic state. We observe that RS is essential for electrically driven magnetization effects and the clear distinction of the two states specifies an opportunity to read out the magnetic state. The isolated $V_{ö}$ do not play any role in RS and magnetic modulations; instead, the Cu^{M+} ions coupled with $V_{ö}$ are essential to tune resistive and magnetic states of the cells by developing the Cu conducting filament. These observations could be helpful to understand and control magnetic modulations of the medium that retain robust $V_{ö}$-related FM.

4. EXPERIMENTAL SECTION

We prepared cell structure from the $Ga_{0.01}Zn_{0.99}O$ and $Cu_{0.04}Zn_{0.96}O$ stoichiometric compositions of the targets (∼99.99% purity) by employing a pulsed KrF excimer laser (λ = 248 nm) with a frequency of 2 Hz and 300 mJ energy. The background pressure of the growth chamber was 1×10^{-4} Pa, and the growth was conducted in the oxygen partial pressure $P(O_2)$ = 0.02 Pa. Prior to growing the thin film structure; we measured the room temperature MH loop of the (001) sapphire crystal substrate to confirm that it was free from magnetic impurity contamination. We first deposited a buffer layer of the $Ga_{0.01}Zn_{0.99}O$ thin film ∼250 nm on the (001) sapphire crystal substrate at 600 °C temperature under $P(O_2)$ = 0.02 Pa. Subsequently, the $Cu_{0.04}Zn_{0.96}O$ layer with a thickness of ∼250 nm was grown on top of the $Ga_{0.01}Zn_{0.99}$/(001) sapphire through shadow-masking to get the sample size of ∼10 mm × 5 mm. For electrical and magnetic measurements, ∼50 nm thick Al metal (∼250 μm diameter) Ohmic contacts were deposited on the surfaces of the $Cu_{0.04}Zn_{0.96}O$ layer with a thermal evaporator to get the final cell structure of Al/$Cu_{0.04}Zn_{0.96}O$/$Ga_{0.01}Zn_{0.99}O$/c-sapphire (inset Figure 1). Resistivity (∼5×10^{-4} Ω cm) and Ohmic behavior of the Al/$Ga_{0.01}Zn_{0.99}O$/sapphire acting as the bottom electrode was carefully checked again. The final single cell size in the present study is ∼250 μm.

The crystal structures were investigated by XRD measurements using a Siemens D5000 diffractometer with the Cu Kα line (0.1541 nm). The film thickness was measured by employing a Hitachi S-4800 field emission scanning electron microscope (FEG). The I−V characteristics were measured by a Keithley Source Meter 2601B. Room temperature magnetic measurements were performed on a Quantum Design SQUID-VSM (Superconducting Quantum Interference Device-Vibrating Sample Magnetometer) with the magnetic field parallel to the film plane. Teflon tweezers were used for sample handling to prevent magnetic contamination. XPS measurements were carried out using a Scienta-Omicron XPS instrument equipped with a microfocused monochromatic Al Kα X-ray source and an Argus Analyzer. The source was operated at 15 keV and with 750 μm spot size, constant analyzer energy of 100 eV for survey scans and 20 eV for high resolution scans. The charge neutralization was applied using a combined low energy to avoid the charging effects, and the XPS data acquisition was performed with Matrix 3.2. Although XPS spot (750 μm) is larger than that of the cell size (∼250 μm), we carefully focused the X-rays on the regions between Al contacts. Data analysis was performed with IGOR Pro by employing XPS fit procedures. The XPS curve fitting was done using the Gaussian−Lorentzian line shape after performing the shrilly background corrections.

AUTHOR INFORMATION

Corresponding Authors

*E-mail: chuhan.pieas@gmail.com (M.Y.).
*E-mail: ccling@hku.hk (F.C.C.L.).

ORCID

Muhammad Younas: 0000-0002-9398-6854

Notes

The authors declare no competing financial interest.

ACKNOWLEDGMENTS

This work was financially supported by the HKSAR RGC GRF (17302115). We are also thankful to PAEC for supporting this work.

REFERENCES

(1) Chen, G.; Song, C.; Chen, C.; Gao, S.; Zeng, F.; Pan, F. Resistive Switching and Magnetic Modulation in Cobalt-Doped ZnO. *Adv. Mater.* **2012**, *24*, 3515−3520.

(2) Matsukura, F.; Tokura, Y.; Ohno, H. Control of magnetism by electric fields. *Nat. Nanotechnol.* **2015**, *10*, 209−220.

(3) Ohno, H.; Chiba, D.; Matsukura, F.; Omiya, T.; Abe, E.; Dietl, T.; Ohno, Y.; Ohtani, K. Electric-field control of ferromagnetism. *Nature* **2000**, *408*, 944−946.

(4) Lottermoser, T.; Lonkai, T.; Amann, U.; Hohlwein, D.; Ihringer, J.; Fiebig, M. Magnetic phase control by an electric field. *Nature* **2004**, *430*, 541−544.

(5) Zou, C.; Wang, H.; Liang, F.; Shao, L. Reversible switching of ferromagnetism in ZnCuO nanorods by electric field. *Appl. Phys. Lett.* **2015**, *106*, 142402−142406.

(6) Wang, X. L.; Shao, Q.; Leung, C. W.; Lortz, R.; Ruotolo, A. Non-volatile, electric control of magnetism in Mn-substituted Zn. *Appl. Phys. Lett.* **2014**, *104*, 062409−062412.

(7) Yang, Y. C.; Pan, F.; Zeng, F.; Liu, M. Switching mechanism transition induced by annealing treatment in nonvolatile Cu/ZnO/Cu/ZnO/Pt resistive memory: From carrier trapping/detrapping to electrochemical metallization. *J. Appl. Phys.* **2009**, *106*, 123705−123709.

(8) Ren, S.-x.; Zhang, L.-y.; Dong, J.-y.; Huang, Y.-f.; Guo, J.-j.; Zhang, L.; Zhao, J.; Zhao, X.; Chen, W. Electric field control of magnetism in Ti/ZnO/Pt and Ti/ZnO/SRO devices. *J. Mater. Chem. C* **2015**, *3*, 4077−4080.

(9) Lin, W.-C.; Chang, P.-C.; Tsai, C.-J.; Shieh, T.-C.; Lo, F.-Y. Voltage-induced reversible changes in the magnetic coercivity of Fe/ZnO heterostructures. *Appl. Phys. Lett.* **2014**, *104*, 062411−062414.

(10) Lin, W.-C.; Chang, P.-C.; Tsai, C.-J.; Hsieh, T.-C.; Lo, F.-Y. Magnetism modulation of Fe/ZnO heterostructure by interface oxidation. *Appl. Phys. Lett.* **2013**, *103*, 212405−212409.

(11) Chang, L.-T.; Wang, C.-Y.; Tang, J.; Nie, T.; Jiang, W.; Chu, C.-P.; Arafin, S.; He, L.; Afsal, M.; Chen, L.-J.; Wang, K. L. Electric-Field Control of Ferromagnetism in Mn-Doped ZnO Nanowires. *Nano Lett.* **2014**, *14*, 1823−1829.

(12) Cheon, D.; Son, M.; Ham, M.-H.; Lee, W. Resistive switching in an amorphous ZnO dielectric film prepared on a Ga-doped ZnO transparent electrode. *RSC Adv.* **2016**, *6*, 103864−103871.

(13) Ma, Q.; Buchholz, D. B.; Chang, R. P. H. Local structures of copper-doped ZnO films. *Phys. Rev. B* **2008**, *78*, 214429−214437.

(14) Herng, T. S.; Wong, M. F.; Qi, D.; Yi, J.; Kumar, A.; Huang, A.; Kartawidjaja, F. C.; Smadici, S.; Abbamonte, P.; Sánchez, H. C.; Shannigrahi, S.; Xue, J. M.; Wang, J.; Feng, Y. P.; Rusydi, A.; Zeng, K.; Ding, J. Mutual Ferromagnetic−Ferroelectric Coupling in Multiferroic Copper-Doped ZnO. *Adv. Mater.* **2011**, *23*, 1635−1640.

DOI: 10.1021/acsomega.7b01192
ACS Omega 2017, 2, 8810−8817

(15) Huang, L. M.; Rosa, A. L.; Ahuja, R. Ferromagnetism in Cu-doped ZnO from first-principles theory. *Phys. Rev. B* **2006**, *74*, 075206−075211.
(16) Rozenberg, M. J.; Inoue, I. H.; Sánchez, M. J. Nonvolatile memory with multilevel switching: a basic model. *Phys. Rev. Lett.* **2004**, *92*, 178302−178305.
(17) Shang, D. S.; Wang, Q.; Chen, L. D.; Dong, R.; Li, X. M.; Zhang, W. Q. Effect of carrier trapping on the hysteretic current-voltage characteristics in $Ag/La_{0.7}Ca_{0.3}MnO_3/Pt$ heterostructures. *Phys. Rev. B* **2006**, *73*, 245427−245433.
(18) Choi, B. J.; Jeong, D. S.; Kim, S. K.; Rohde, C.; Choi, S.; Oh, J. H.; Kim, H. J.; Hwang, C. S.; Szot, K.; Waser, R.; Reichenberg, B.; Tiedke, S. Resistive switching mechanism of TiO_2 thin films grown by atomic-layer deposition. *J. Appl. Phys.* **2005**, *98*, 033715−033724.
(19) Waser, R.; Aono, M. Nanoionics-based resistive switching memories. *Nat. Mater.* **2007**, *6*, 833−840.
(20) Yang, Y. C.; Pan, F.; Liu, Q.; Liu, M.; Zeng, F. Fully Room-Temperature-Fabricated Nonvolatile Resistive Memory for Ultrafast and High-Density Memory Application. *Nano Lett.* **2009**, *9*, 1636−1643.
(21) Younas, M.; Shen, J.; He, M.; Lortz, R.; Azad, F.; Akhtar, M. J.; Maqsood, A.; Ling, F. C. C. Role of multivalent Cu, oxygen vacancies and CuO nanophase in the ferromagnetic properties of ZnO: Cu thin films. *RSC Adv.* **2015**, *5*, 55648−55657.
(22) Das, B. C.; Batabyal, S. K.; Pal, A. J. A Bit per Particle: Electrostatic Assembly of CdSe Quantum Dots as Memory Elements. *Adv. Mater.* **2007**, *19*, 4172−4176.
(23) Wang, X. B.; Li, D. M.; Zeng, F.; Pan, F. Microstructure and properties of Cu-doped ZnO films prepared by dc reactive magnetron sputtering. *J. Phys. D: Appl. Phys.* **2005**, *38*, 4104−4108.
(24) Kanai, Y. Admittance Spectroscopy of Cu-Doped ZnO Crystals. *Jpn. J. Appl. Phys.* **1991**, *30*, 703−707.
(25) McCluskey, M. D.; Jokela, S. J. Defects in ZnO. *J. Appl. Phys.* **2009**, *106*, 071101−071113.
(26) Rahman, M. A.; Westerhausen, M. T.; Nenstiel, C.; Choi, S.; Hoffmann, A.; Gentle, A.; Phillips, M. R.; Ton-That, C. Charge state switching of Cu acceptors in ZnO nanorods. *Appl. Phys. Lett.* **2017**, *110*, 121907−121910.
(27) Zeghbroeck, B. V. Principles of Semiconductor Devices; University of Colorado: Boulder CO, 2006.
(28) Kaidashev, E. M.; Lorenz, M.; von Wenckstern, H.; Rahm, A.; Semmelhack, H.-C.; Han, K.-H.; Benndorf, G.; Bundesmann, C.; Hochmuth, H.; Grundmann, M. High electron mobility of epitaxial ZnO thin films on c-plane sapphire grown by multistep pulsed-laser deposition. *Appl. Phys. Lett.* **2003**, *82*, 3901−3903.
(29) Moulder, J. F.; Stickle, W. F.; Sobol, P. E.; Bomben, K. D. *Handbook of X-ray Photoelectron Spectroscopy*; Perkin-Elmer: Eden Prairie, 1992.
(30) Chakraborti, D.; Narayan, J.; Prater, J. T. Room temperature ferromagnetism in $Zn_{1-x}Cu_xO$ thin films. *Appl. Phys. Lett.* **2007**, *90*, 062504−06206.
(31) Kim, J. B.; Byun, D.; Ie, S. Y.; Park, D. H.; Choi, W. K.; Choi, J.-W.; Angadi, B. Cu-doped ZnO-based p−n hetero-junction light emitting diode. *Semicond. Sci. Technol.* **2008**, *23*, 095004−095009.
(32) Sohn, J.; Song, S.-H.; Nam, D.-W.; Cho, I.-T.; Cho, E.-S.; Lee, J.-H.; Kwon, H.-I. Effects of vacuum annealing on the optical and electrical properties of p-type copper-oxide thin-film transistors. *Semicond. Sci. Technol.* **2013**, *28*, 015005−015009.
(33) Peng, H. Y.; Li, G. P.; Ye, J. Y.; Wei, Z. P.; Zhang, Z.; Wang, D. D.; Xing, G. Z.; Wu, T. Electrode dependence of resistive switching in Mn-doped ZnO: Filamentary versus interfacial mechanisms. *Appl. Phys. Lett.* **2010**, *96*, 192113−192115.
(34) Kukreja, L. M.; Misra, P.; Fallert, J.; Phase, D. M.; Kalt, H. Correlation of spectral features of photoluminescence with residual native defects of ZnO thin films annealed at different temperatures. *J. Appl. Phys.* **2012**, *112*, 013525−013534.
(35) Zhang, J.; Yang, H.; Zhang, Q.-L.; Dong, S.; Luo, J. K. Structural, optical, electrical and resistive switching properties of ZnO thin films deposited by thermal and plasma-enhanced atomic layer deposition. *Appl. Surf. Sci.* **2013**, *282*, 390−395.
(36) Tang, M. H.; Jiang, B.; Xiao, Y. G.; Zeng, Z. Q.; Wang, Z. P.; Li, J. C.; He, J. Top electrode-dependent resistance switching behaviors of ZnO thin films deposited on Pt/Ti/SiO2/Si substrate. *Microelectron. Eng.* **2012**, *93*, 35−38.
(37) Chang, W.-Y.; Lai, Y.-C.; Wu, T.-B.; Wang, S.-F.; Chen, F.; Tsai, M.-J. Unipolar resistive switching characteristics of ZnO thin films for nonvolatile memory applications. *Appl. Phys. Lett.* **2008**, *92*, 022110−022112.

DOI: 10.1021/acsomega.7b01192
ACS Omega 2017, 2, 8810−8817